

A Wing-Body Fairing Design for the DLR-F6 Model: A DPW-III Case Study

John C. Vassberg^{}, Anthony J. Sclafani[†], Mark A. DeHaan[‡]*

The Boeing Company
Phantom Works
Huntington Beach, CA 92647

ABSTRACT

The work presented herein has been performed in preparation of the Third AIAA CFD Drag Prediction Workshop to be held June, 2006 at the AIAA 24th Applied Aerodynamics conference in San Francisco, California. The purpose of this work is to provide a new test case to address a problematic issue related to the inability for the industry-wide state-of-the-art CFD to achieve asymptotic grid convergence for cases with moderate-to-large amounts of flow separation. Two wing-body fairings have been designed for the DLR-F6 model geometry. The first fairing greatly alleviates the side-of-body separation near the wing upper-surface trailing-edge, while the second fairing has completely removed this separation bubble. These geometries will be made available for public release, although only the second fairing will be a subject of study in the next workshop.

INTRODUCTION

In recent years, the AIAA CFD Drag Prediction Workshop (DPW) series has been an instrumental aid for the CFD community to assess its state-of-the-art (SOA). This international workshop provides an impartial forum for research scientists, engineers, designers, and developers from industry, academia and government laboratories to gather and discuss results of very specific test cases defined by the DPW Organizing Committee (OC). The OC provides a set of mandatory test cases, complete with baseline grids, for voluntary participants to analyze and report on at the workshops. The over-whelming response by participants/attendees has been very positive and provides the impetus to continue and further expand this workshop series. The database of CFD calculations performed to date has yielded insight into issues which must be addressed through further research. To facilitate progress, these test cases, grids, and CFD results are made available to the public domain through the DPW website, Reference [1].

The first DPW (DPW-I) was held June 2001 in Anaheim, California. DPW-I invited several papers to the 40th AIAA Aerospace Sciences Meeting (ASM) in Reno, NV, January 2004, see References [1-7]. The subject under study was the DLR-F4 wing-body (WB) configuration, (commercial transport-class aircraft). Wind tunnel data and a comprehensive description for this model is available through AGARD, Reference [8].

^{*} AIAA Associate Fellow, Boeing Technical Fellow

[†] Senior Engineer

[‡] Principal Engineer

DPW-I clearly quantified that the scatter of CFD drag prediction is much larger than that required by industry.

The second DPW (DPW-II) was held June 2003 in Orlando, Florida. DPW-II hosted two sessions at the 42nd ASM in Reno, NV, January 2004, see References [9-23]. The DLR-F6 WB and wing-body-nacelle-pylon (WBNP) geometries were the configurations under study. These geometries exhibit large regions of flow separation at cruise conditions. Specifically, there is a pocket of flow separation at the side-of-body (SOB) near the wing upper-surface trailing-edge; there is a full-span separation at the wing upper-surface trailing-edge; there is shock-induced separation on the inboard-side of the pylon in the channel flow between the wing lower-surface and the nacelle. Figure 1 provides the composite DPW-II drag polars for the WB test case. The scatter band of these SOA CFD predictions spans 20-30 counts of drag. Figure 2 provides a representative result from the DPW-II grid-convergence study. Note that asymptotic grid convergence (AGC) has not been achieved in these data. In general, almost all participant results failed to demonstrate AGC. The consensus of the DPW-II attendees as well as the post-workshop panel discussions at the ASM was that the primary cause that AGC is not achieved is the excessive amount of flow separation that exists about the DLR-F6 model. As a consequence, the CFD community requested the OC to provide test cases that will help quantify how much and what types of flow separation the SOA CFD methods can accommodate and still exhibit AGC. The OC has decided to establish test cases for DPW-III that will be based on the DLR-F6 model, yet will systematically reduce the level of flow separation inherent with this configuration. This includes reducing the wing upper-surface trailing-edge flow separation by increasing the Reynolds number of a test case and addressing the SOB juncture flow. To this end, the authors have developed two WB fairings for the DLR-F6 model. The following section describes this geometry build-up.

WING-BODY FAIRING GEOMETRY

This section describes the geometry build-up of two new WB fairings for the DLR-F6 model. When this work was initiated, the goal was to develop a fairing that will greatly alleviate the size of the SOB separation bubble, and another that will provide fully-attached flow at the SOB. Figures 3-5 depict the baseline DLR-F6 wing-body geometry; note that only a portion of the wing-root section is included in these images. In Figure 5, the view from behind the model shows an acute included-angle between the fuselage and wing upper-surface. This angle is about 60° and causes the associated juncture flow to separate.

To help alleviate the SOB separation, a fairing designated FX1 has been developed. This fairing is shown relative to the baseline geometry in Figures 6-9. One criterion of the design of FX1 is to ensure that the fairing surface is everywhere outside or tangent to the baseline fuselage. The purpose of this constraint is to help facilitate possible future wind-tunnel testing of the DLR-F6 model by not explicitly requiring that the original fuselage geometry be modified. Figures 6-7 might indicate that the FX1 part intersects and “penetrates” into the fuselage; however, this is not the case. Rather, this optical illusion is an artifact of the hidden-line program used to create these images; the

perimeter of the FX1 geometry is precisely coincident with the fuselage surface. The rear view visual of Figure 9 shows that the included-angle at the SOB has been increased to a value of about 90° . Furthermore, the FX1 fairing has partially filled in this problematic region such that direction of the juncture flow no longer has a significant span-wise component. These design features improve the health of the SOB viscous boundary layer.

To provide fully-attached flow at the SOB juncture, another fairing designated FX2 has been developed. The design of the FX2 fairing is built starting with the FX1 geometry and adding a bump centered near the wing trailing-edge. This bump is everywhere outside or tangent to the FX1 surface. Again, this criterion is motivated by possible future wind-tunnel tests of the DLR-F6 model. The FX2 geometry is depicted in Figures 10-13. Figure 10 shows that the FX2 blister does not make contact with the baseline fuselage. Figures 11-12 provide the relative positions between the FX2 bump and the FX1 fairing. Figure 13 is a three-view of the SOB region. Note that the rear and top views of this figure show how the FX2 bump further fills in this problematic region.

Several criteria were implemented during the design of the FX1 and FX2 fairings. This includes the aforementioned considerations for possible future wind-tunnel testing. In addition, these geometries are developed without application of company proprietary design procedures to be certain that they can be distributed into the public domain. The primary goal of the FX2 design is to provide fully-attached SOB flow at cruise conditions; no consideration was given during this development effort to minimize drag or to be compatible with the high-lift system of a real aircraft. Finally, the geometry definition is to be provided to the public domain in several formats. To ensure that these definitions are mathematically equivalent, the geometries have been post-processed by Laflin and Zickuhr of Cessna Aircraft by developing a CATIA model and exporting IGES and STEP formats. The designation of the post-processed geometry is FX2B. All three format definitions will be available in the near term.

The next section provides flow solutions about the baseline, FX1, and FX2B configurations at the DLR-F6 cruise conditions. These results demonstrate that the objectives of the two fairing designs were accomplished.

FLOW SOLUTIONS

This section verifies that the design goals of the FX1 and FX2B fairings have been met. NASA's OVERFLOW CFD method is utilized in this study to assess the aerodynamic characteristics of the subject configurations. This SOA CFD method is based on the Reynolds-Averaged Navier-Stokes (RANS) equations. Eddy viscosity equations are closed with various turbulence models. RANS equations are solved using three levels of grid sequencing, multigrid acceleration, and local time stepping to converge to a steady-state solution. Grid sequencing adopted herein uses 300 iterations in the coarse and intermediate grids, 1000 iterations in the fine mesh, followed by an update on angle-of-attack, and a final 1000 iterations in the fine mesh. The angle-of-attack update is needed to converge the solution to a specified lifting condition. Cruise condition for the DLR-F6 model is 0.75 Mach number and $C_L = 0.5$. Wind-tunnel Reynolds number for this model is 3 million, based on reference chord. The overset grid is comprised of 6.8 million nodes and 12 zones; it was developed using ZONI3G, OVERGRID, and PEGASUS 5.

Related specifically to the application of the OVERFLOW code, past experience provides insight into which turbulence models work best with which difference stencils for transonic turbulent flows. In this design study, the combination of the Baldwin-Barth turbulence model and a central-difference-stencil is utilized as it provides a solution that is most prone to flow separation; we caution that this is not necessarily the most accurate approach. However, designing for fully-attached flows with this combination should minimize the chance that other SOA CFD methods will yield a solution with separation; at least this is the authors' intent. Hence, solutions provided in this section are all based on the Baldwin-Barth / central-difference combination.

Figures 14-16 provide isometric views of the SOB region looking from above and behind the wing trailing-edge for the baseline, FX1, and FX2B geometries, respectively. The surface pressures are provided with a color map where dark blue indicates stagnation ($C_p=1.0$), green is freestream ($C_p=0.0$), and bright red shows accelerated flow ($C_p=-1.0$). A shock exists where red and yellow meet. The "surface" streamlines depicted in these figures are actually streamlines confined to a computational plane ($L=5$) located just off the no-slip surface.

Figure 14 illustrates the large SOB separation pocket of the baseline DLR-F6 WB configuration. This image also confirms that beyond the bubble, a trailing-edge separation persists out the span of the wing. Figure 15 indicates that the size of the SOB separation bubble has been greatly diminished with inclusion of the FX1 fairing on the baseline DLR-F6 wing-body configuration. Figure 16 verifies that the FX2B bump-fairing provides fully-attached flow at the SOB. This figure also indicates that the FX2B fairing had very little impact on the full-span trailing-edge separation. Hence, all goals of this design exercise have been achieved. For completeness, a comparison of the SOB C_p distributions is provided in Figure 17 at semi-span stations of 15.4%, 18.8%, and 22.2%. Note that the angle-of-attack for the baseline configuration is about 0.25° higher than that of either of the filleted geometries for the constant lifting condition of $C_L=0.5$.

Figures 18-21 give the convergence histories of the OVERFLOW solutions for all three cases. Figure 18 provides the convergence of residuals. In this graph, the spikes at 300 and 600 iterations are due to the grid sequencing to the next finer mesh. The spike at 1600 iterations is caused by the angle-of-attack adjustment. Notice that the residual for the baseline geometry stalls at about 3 orders-of-magnitude reduction, while that for the FX1 case fluctuates around 5.25 orders-of-magnitude reduction. The residual history for the fully-attached FX2B case is very well behaved, has achieved a reduction of over 6.5 orders, and has established an asymptotic convergence rate on the fine mesh. Although AGC has not yet been confirmed, this is a very encouraging result as this flow field does contain the full-span wing upper-surface trailing-edge separation.

Figures 19-21 provide the convergence histories of lift, drag, and pitching moment, respectively. In all of these plots, the baseline convergence is characterized as terminating with an oscillatory limit cycle. Note that the "converged" pitching moment of the baseline is about 0.01 higher than that for the FX1 and FX2B cases. Also, the lift history for the FX1 geometry appears to be creeping slightly upward near the end of the solution; this might be an indication that its small SOB flow separation pocket is slowly reducing in size as the solution converges. The convergence histories for the FX2B design are all very well behaved.

SUMMARY

Two wing-body fairings have been designed for the DLR-F6 model to address the SOB pocket of flow separation. The first fairing, FX1, greatly alleviates the SOB bubble, while the second design, FX2B, provides fully-attached flow at the SOB. The convergence histories for the FX2B geometry are all well behaved; residuals drop 6.5 orders and establish an asymptotic convergence rate. These designs are developed with consideration for possible future wind-tunnel testing, and to ensure that the geometries can be placed into the public domain. All goals for this design effort have been achieved.

ACKNOWLEDGEMENTS

The authors thank Boeing Phantom Works – Huntington Beach for funding this design effort. We also acknowledge the support of various other institutions that have made the Drag Prediction Workshop series the success that it is. This includes AIAA Headquarters for helping the OC facilitate the workshops, and the AIAA Applied Aerodynamics Technical Committee for sponsoring the workshops. For providing membership on the OC, we commend The Boeing Company, Cessna Textron, National Aeronautics and Space Administration, University of Wyoming, DLR-Germany, and ONERA-France.

REFERENCES

1. URL: <http://ad-www.larc.nasa.gov/tsab/cfdlarc/aiaa-dpw>
email: dpw@cessna.textron.com
2. DW Levy, JC Vassberg, RA Wahls, T Zickuhr, S Pirzadeh, MJ Hemsch, “Summary of Data from the First AIAA CFD Drag Prediction Workshop,” AIAA Paper 2002-0841, Reno, NV, January, 2001.
3. JC Vassberg, PG Buning, CL Rumsey, “Drag Prediction for the DLR-F4 Wing/Body using OVERFLOW and CFL3D on an Overset Mesh,” AIAA Paper 2002-0840, 40th AIAA ASM, Reno, NV, January, 2002.
4. SZ Pirzadeh, “Assessment of the Unstructured Grid Software TetrUSS for Drag Prediction of the DLR-F4 Configuration,” AIAA Paper 2002-0839, Reno, NV, January, 2001.
5. DJ Mavriplis, DW Levy, “Transonic Drag Prediction using an Unstructured Multigrid Solver,” AIAA Paper 2002-0838, Reno, NV, January, 2001.
6. M Rakowitz, et. al., “Structured and Unstructured Computations on the DLR-F4 Wing-Body Configuration,” AIAA Paper 2002-0837, Reno, NV, January, 2001.
7. M Hemsch, “Statistical Analysis of CFD Solutions from the Drag Prediction Workshop,” AIAA Paper 2002-0842, Reno, NV, January, 2001.
8. G Redeker, “DLR-F4 Wing-Body Configuration,” *A Selection of Experimental Test Cases for the Validation of CFD Codes*, AGARD Report AR-303, August, 1994.

9. KR Laflin, SM Klausmeyer, T Zickuhr, JC Vassberg, RA Wahls, JH Morrison, O Brodersen, M Rakowitz, EN Tinoco, JL Godard, "Summary of Data from the Second AIAA CFD Drag Prediction Workshop," AIAA Paper 2004-0555, 42nd AIAA ASM, Reno, NV, January, 2004.
10. N Pfeiffer, "Reflections on the Second Drag Prediction Workshop," AIAA Paper 2004-0557, Reno, NV, January, 2004.
11. M Hemsch, J Morrison, "Statistical Analysis of CFD Solutions from the 2nd Drag Prediction Workshop," AIAA Paper 2004-0556, Reno, NV, January, 2004.
12. E Lee-Rausch, N Frink, W Milholen, D Mavriplis, "Transonic Drag Prediction using Unstructured Grid Solvers," AIAA Paper 2004-0554, Reno, NV, January, 2004.
13. S Klausmeyer, "Drag, Lift, and Moment Estimates for Transonic Aircraft using the Navier-Stokes Equations," AIAA Paper 2004-0553, Reno, NV, January, 2004.
14. E Tinoco, T Su, "Drag Prediction with the Zeus/CFL3D System," AIAA Paper 2004-0552, Reno, NV, January, 2004.
15. K Yamamoto, "CFD Sensitivity to Drag Prediction on DLR-F6 Configuration by Structured Method and Unstructured Method," AIAA Paper 2004-0398, Reno, NV, January, 2004.
16. Y Kim, S Park, J Kwon, "Drag Prediction of DLR-F6 using the Turbulent Navier-Stokes Calculations with Multigrid," AIAA Paper 2004-0397, Reno, NV, January, 2004.
17. G May, E van der Weide, A Jameson, S Shankaran, "Drag Prediction of the DLR-F6 Configuration," AIAA Paper 2004-0396, Reno, NV, January, 2004.
18. K Wutzler, "Aircraft Drag Prediction using Cobalt," AIAA Paper 2004-0395, Reno, NV, January, 2004.
19. C Rumsey, S Rivers, J Morrison, "Study of CFD Variation on Transport Configurations from the Second Drag-Prediction Workshop," AIAA Paper 2004-0394, Reno, NV, January, 2004.
20. AJ Sclafani, MA DeHaan, JC Vassberg, "OVERFLOW Drag Prediction for the DLR-F6 Transport Configuration: A DPW-II Case Study," AIAA Paper 2004-0393, 42nd AIAA ASM, Reno, NV, January, 2004.
21. R Langtry, M Kuntz, F Menter, "Drag Prediction of Engine-Airframe Interference Effects with CFX-5," AIAA Paper 2004-0392.
22. O Brodersen, M Rakowitz, S Amant, D Destarac, M Sutcliffe, "Airbus, ONERA, and DLR Results from the 2nd AIAA Drag Prediction Workshop," AIAA Paper 2004-0391.
23. JC Vassberg, MA DeHaan, AJ Sclafani, "Grid Generation Requirements for Accurate Drag Predictions based on OVERFLOW Calculations," AIAA Paper 2003-4124, 16th AIAA Applied Aerodynamics Conference, Orlando, FL, June, 2003.

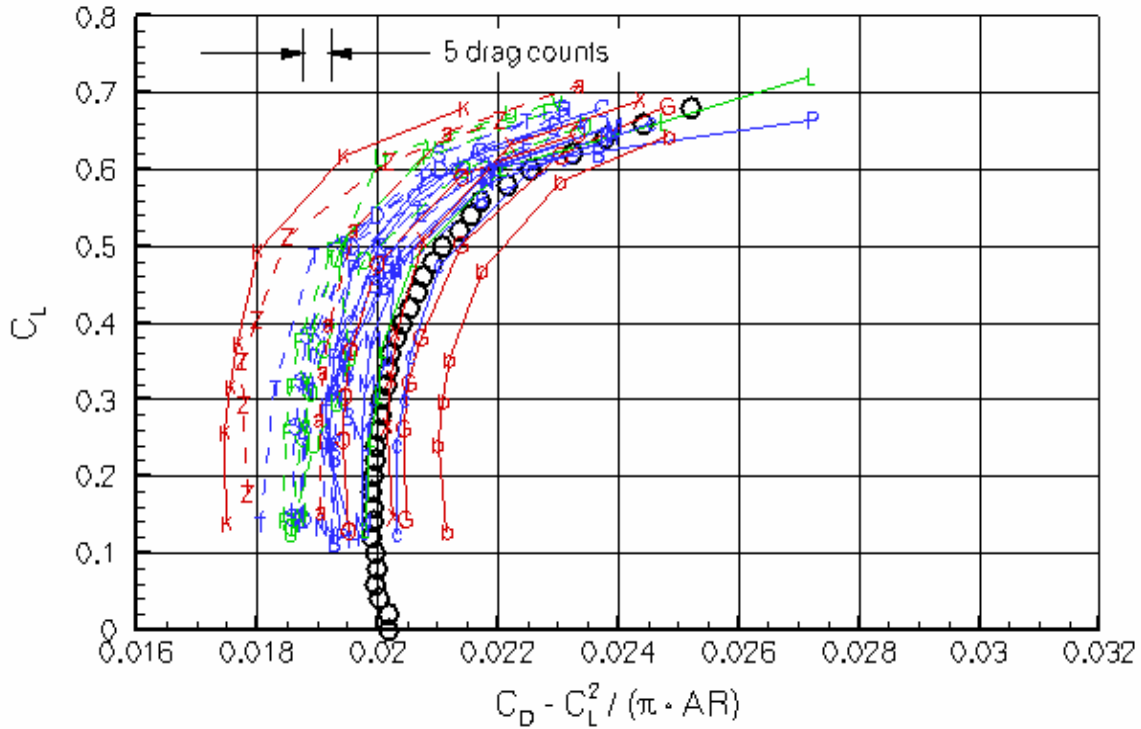


Figure 1: DLR-F6 Wing-Body Drag Polar Results from the DPW-II.

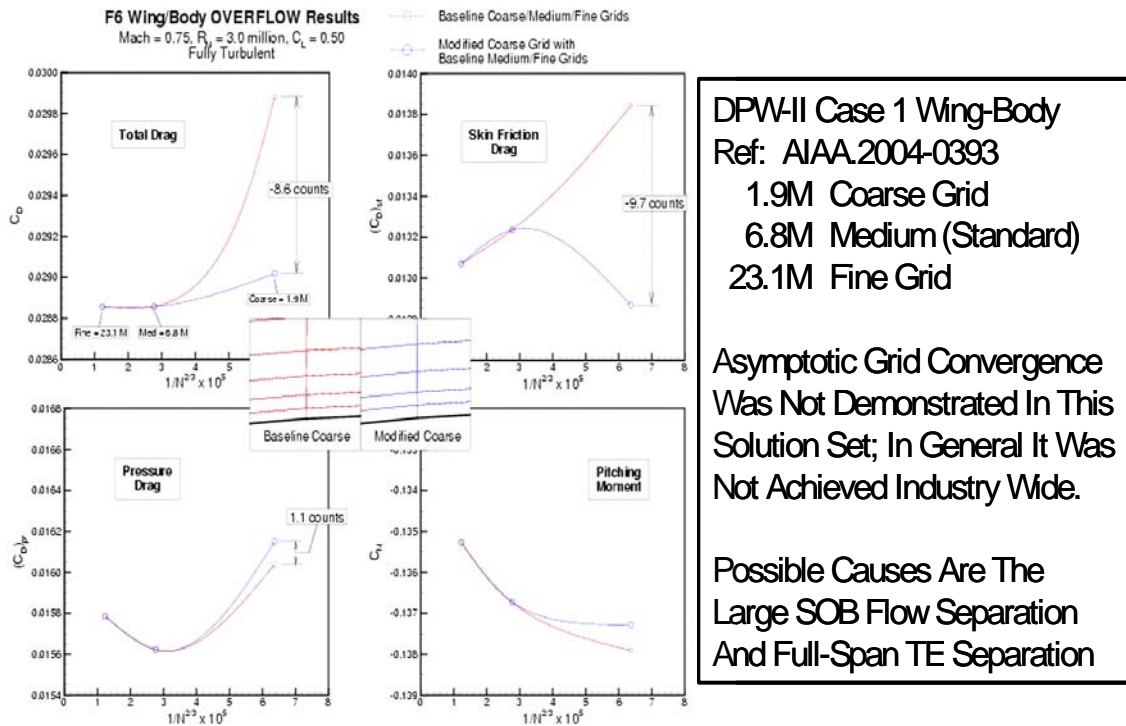


Figure 2: Sample Grid Convergence Study from the DPW-II.

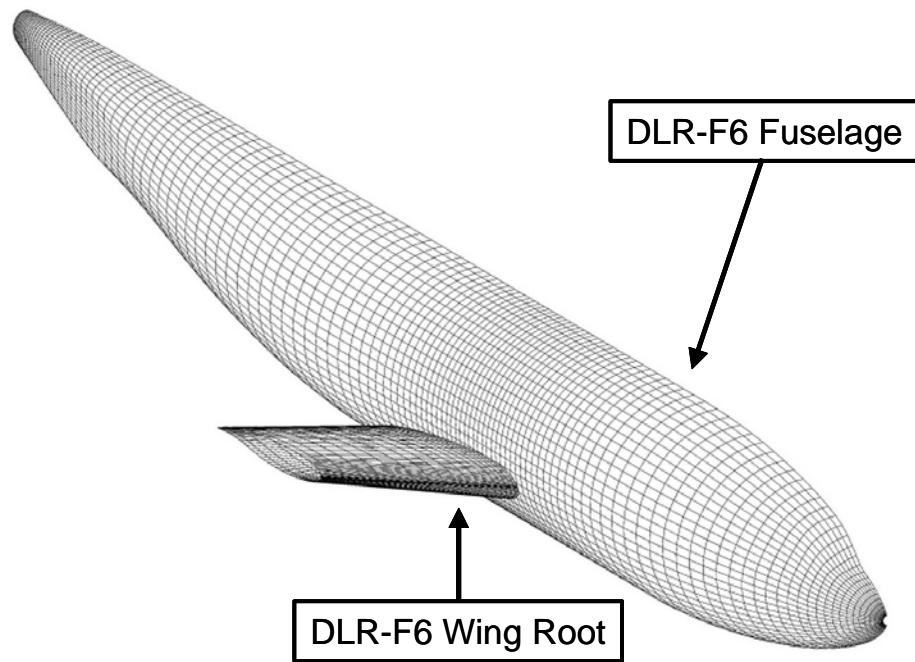


Figure 3: Isometric View of Baseline DLR-F6 Fuselage with a Section of the Wing Root.

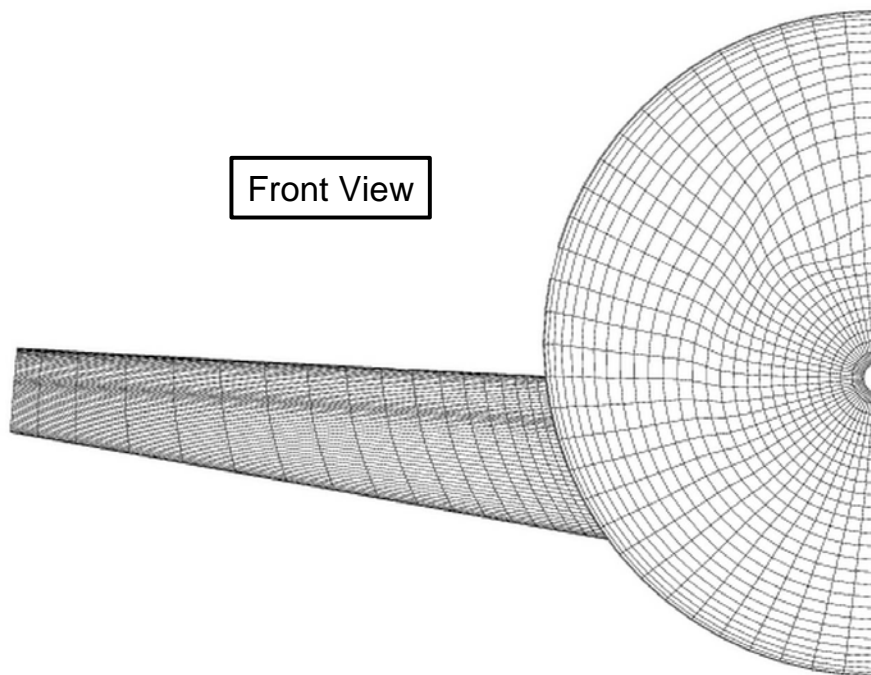


Figure 4: Front View of Baseline DLR-F6 Fuselage with a Section of the Wing Root.

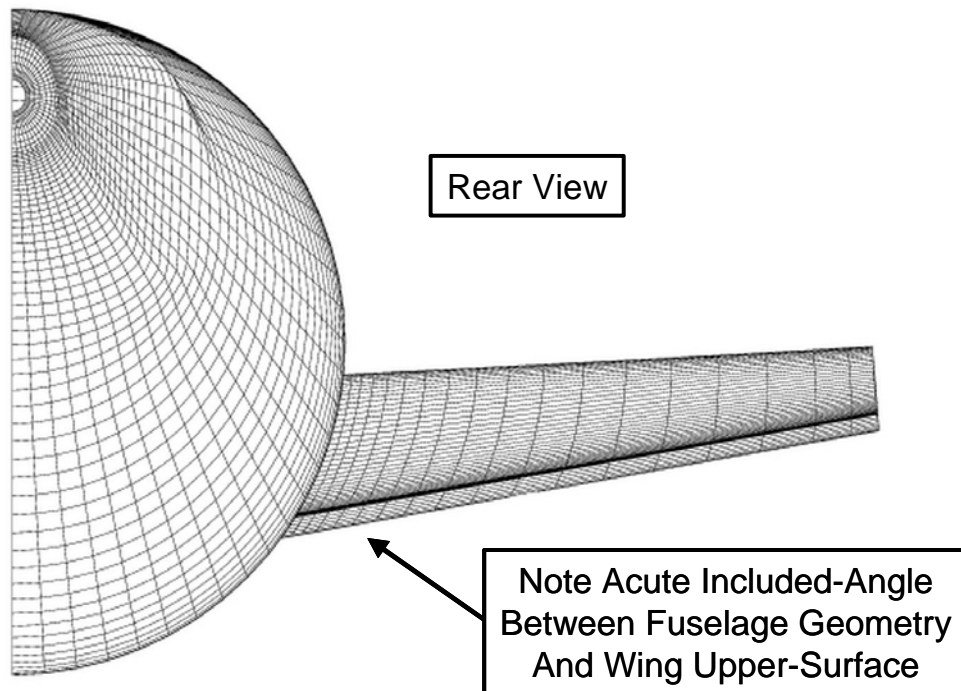


Figure 5: Rear View of Baseline DLR-F6 Fuselage with a Section of the Wing Root.

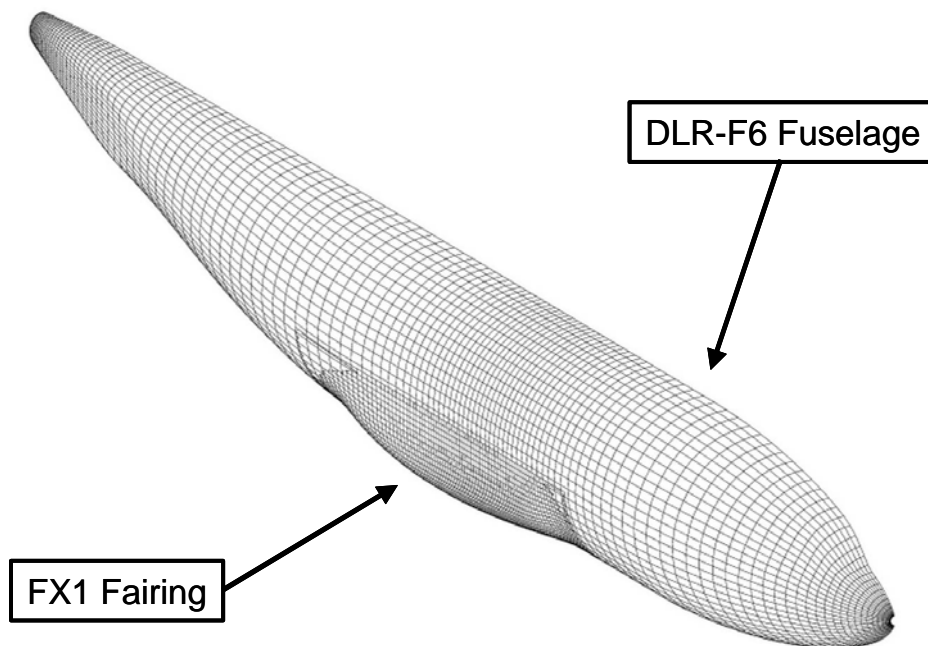


Figure 6: Isometric View of Baseline DLR-F6 Fuselage with FX1 WB Fairing.

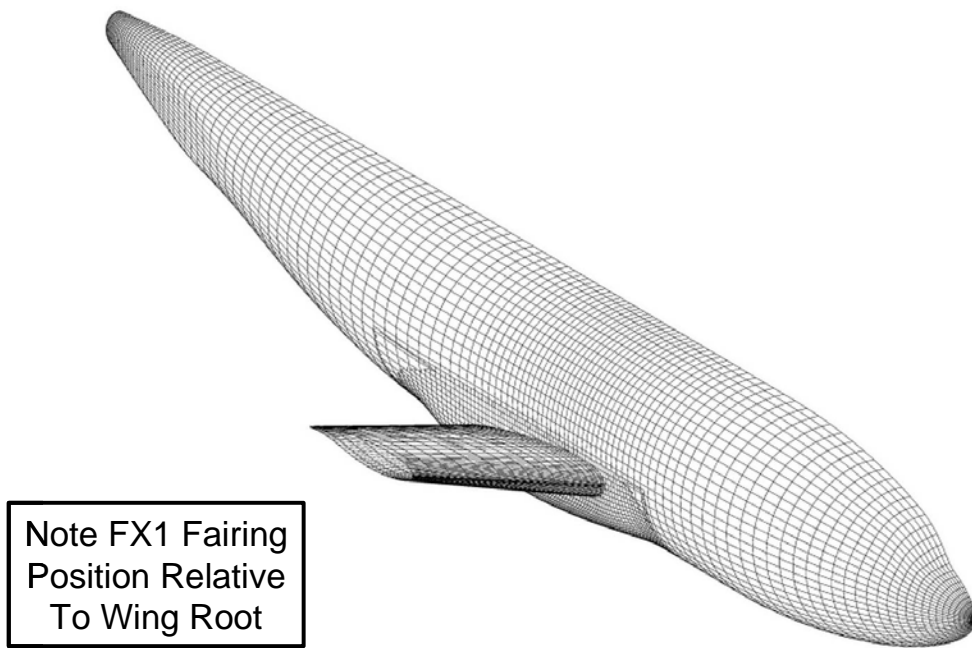


Figure 7: Isometric View of Baseline DLR-F6 Fuselage with FX1 WB Fairing.

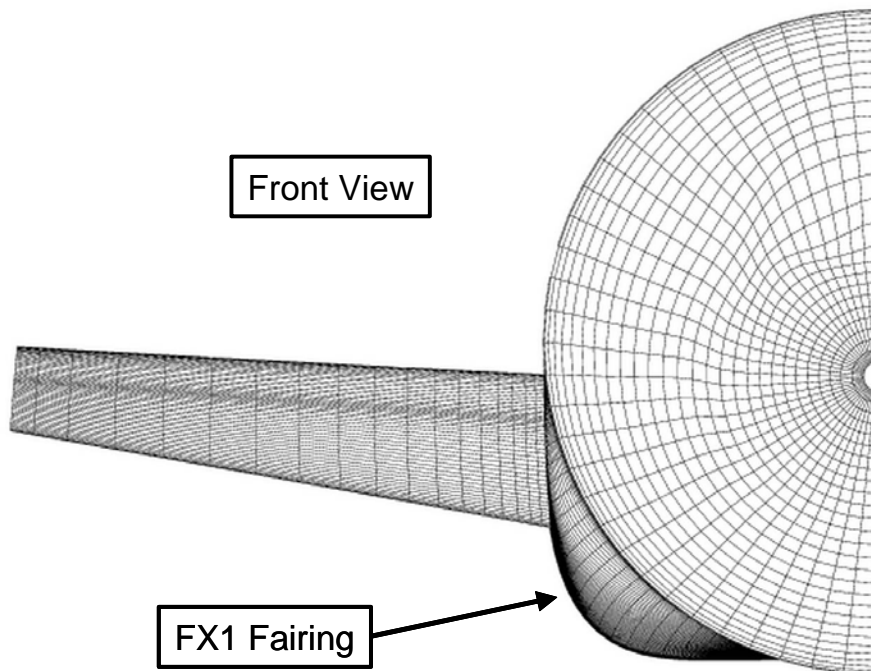


Figure 8: Front View of Baseline DLR-F6 Fuselage with FX1 WB Fairing.

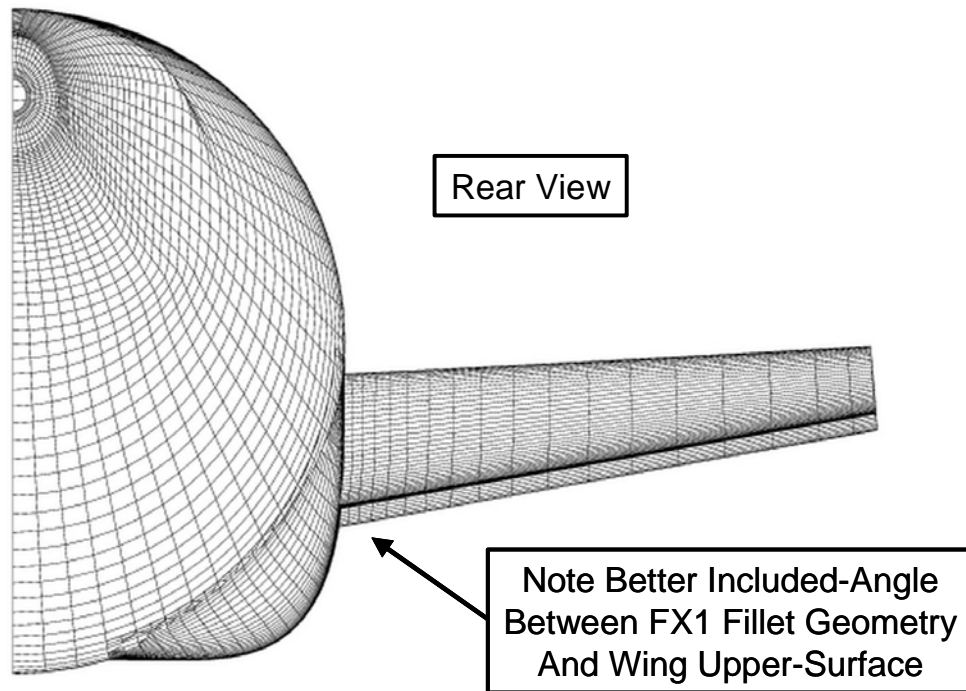


Figure 9: Rear View of Baseline DLR-F6 Fuselage with FX1 WB Fairing.

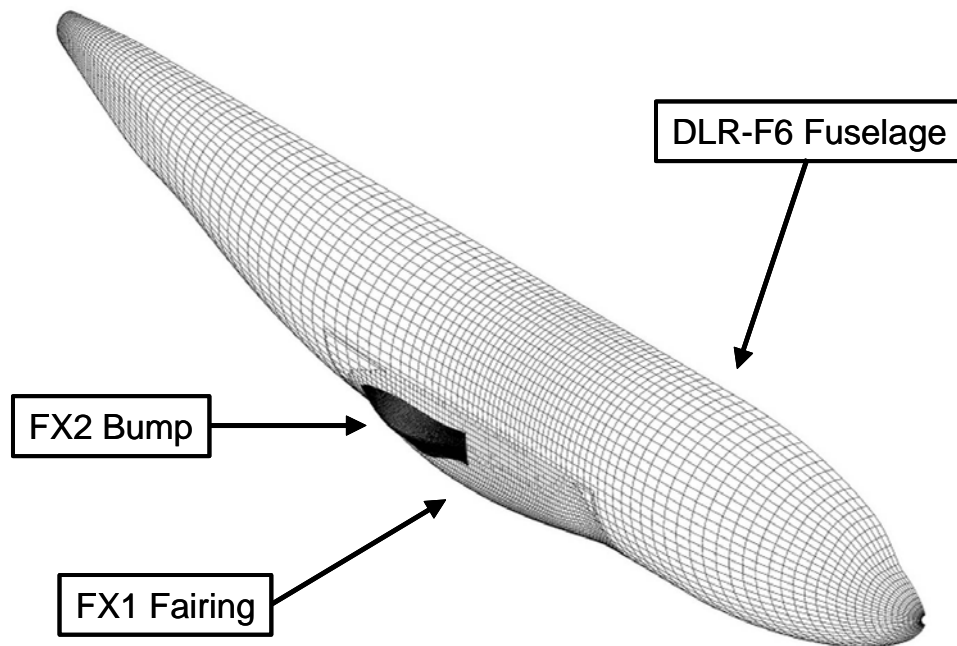


Figure 10: Isometric View of Baseline DLR-F6 Fuselage with FX2 WB Bump-Fairing.

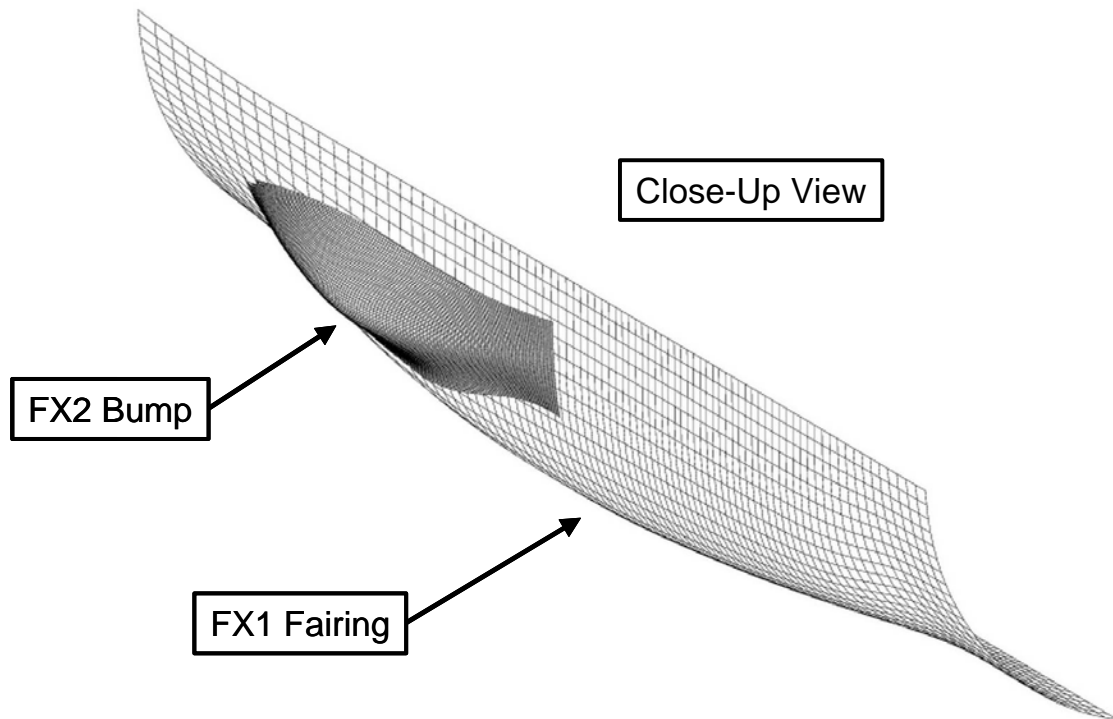


Figure 11: Close-Up View of Baseline DLR-F6 Fuselage with FX2 WB Bump-Fairing.

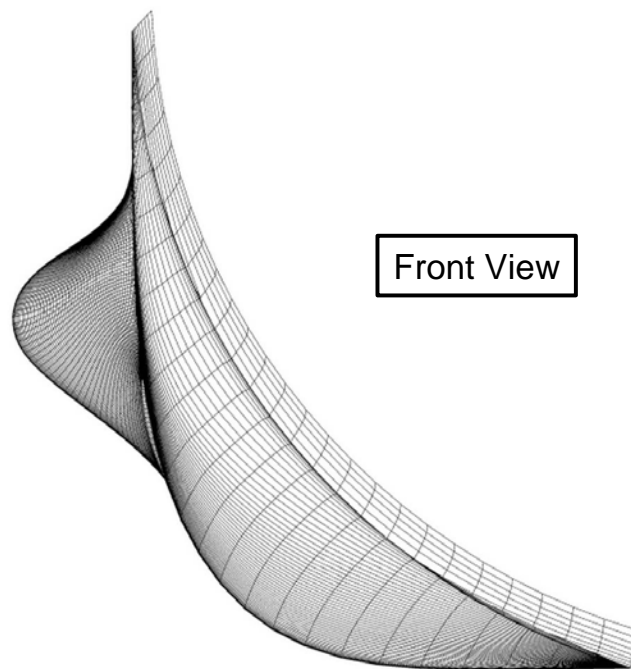


Figure 12: Front View of Baseline DLR-F6 Fuselage with FX2 WB Bump-Fairing.

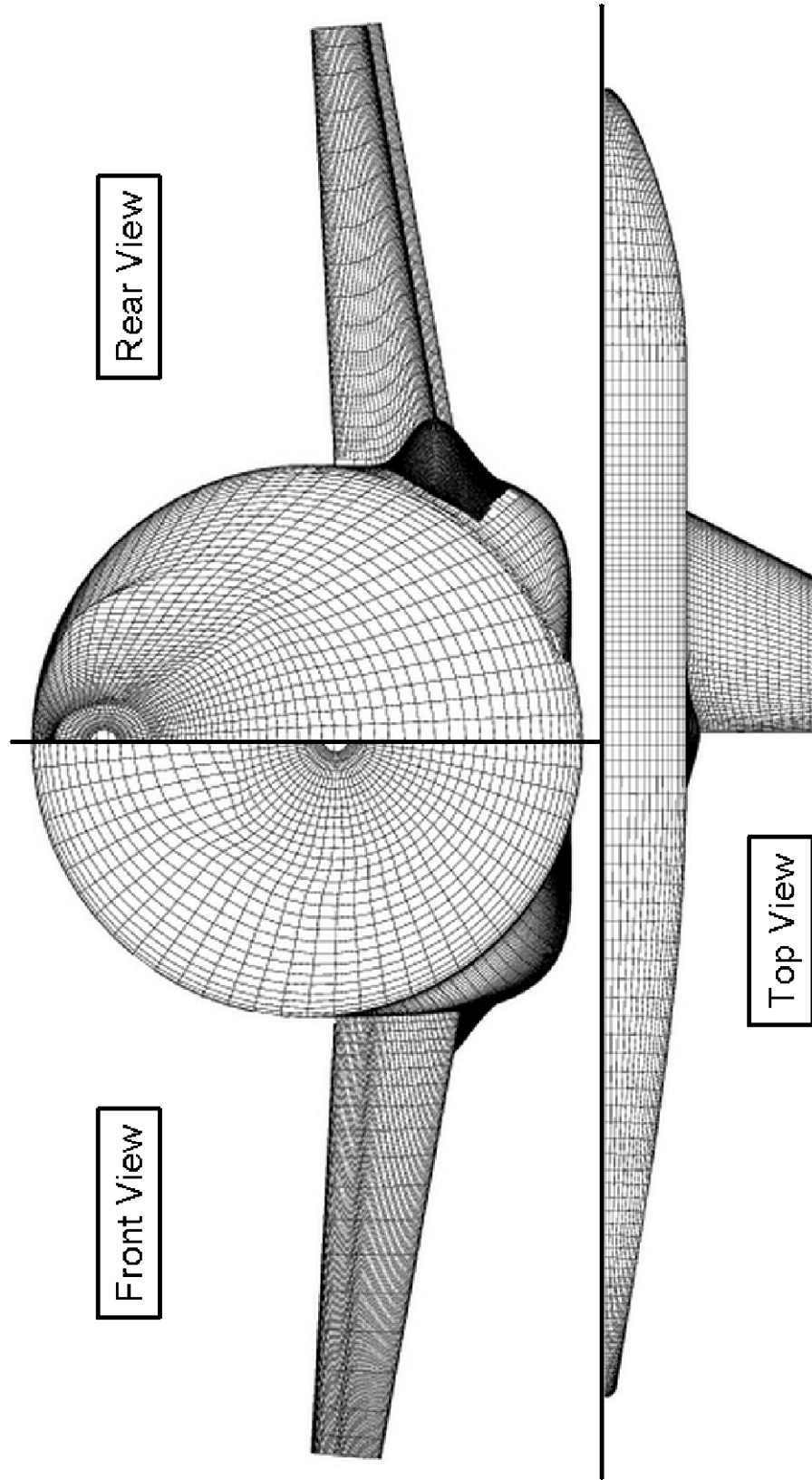


Figure 13: Three-View of Baseline DLR-F6 Fuselage with FX2 WB Bump-Fairing.

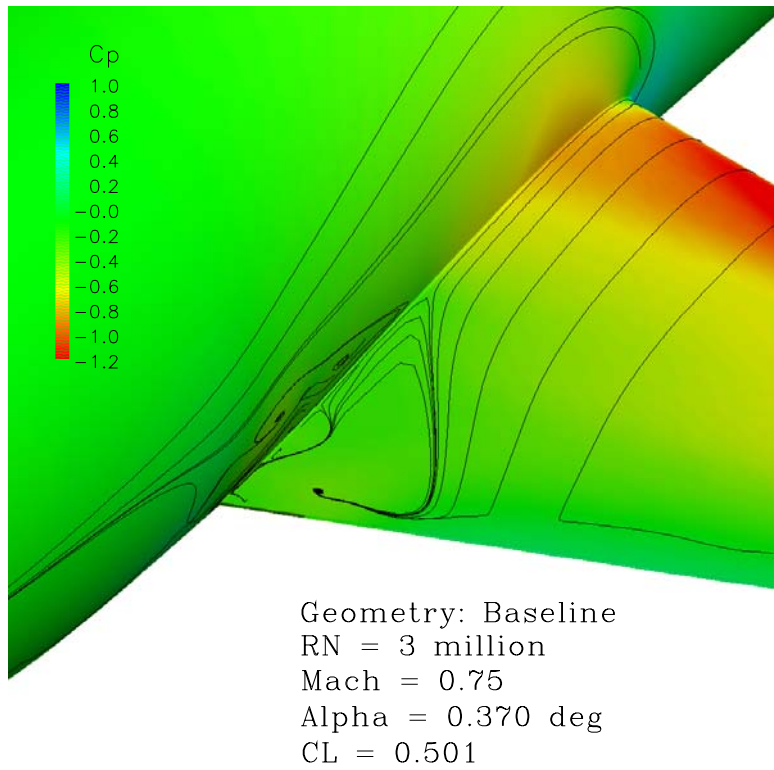


Figure 14: Baseline DLR-F6 Wing-Body Surface Streamlines

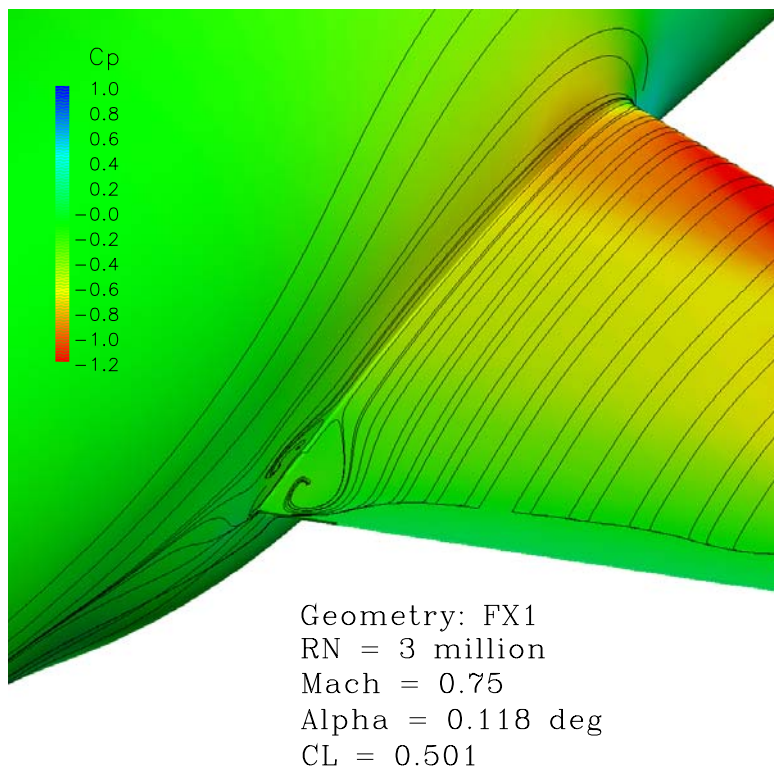


Figure 15: DLR-F6 Wing-Body-FX1 Surface Streamlines

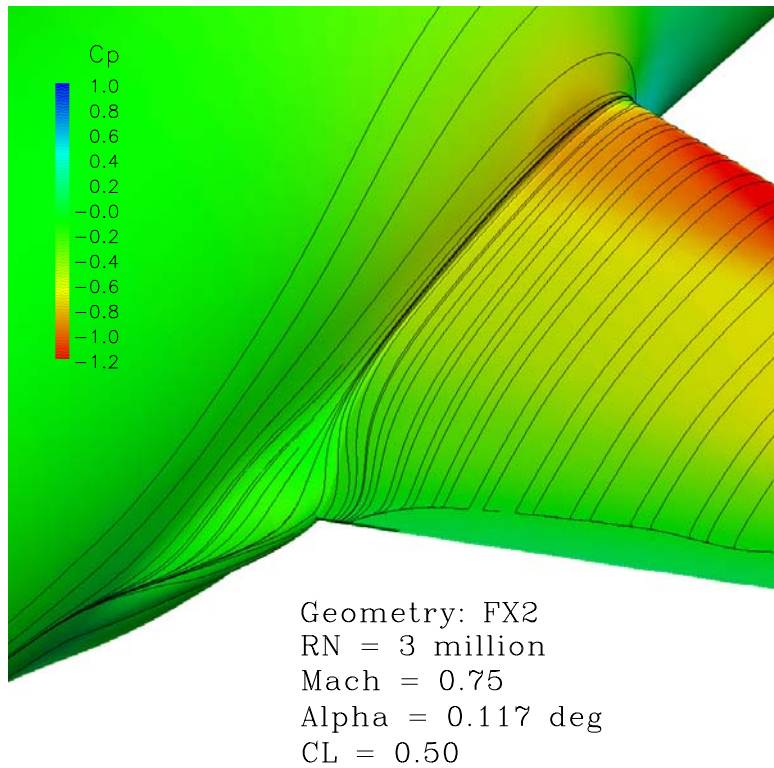


Figure 16: DLR-F6 Wing-Body-FX2 Surface Streamlines.

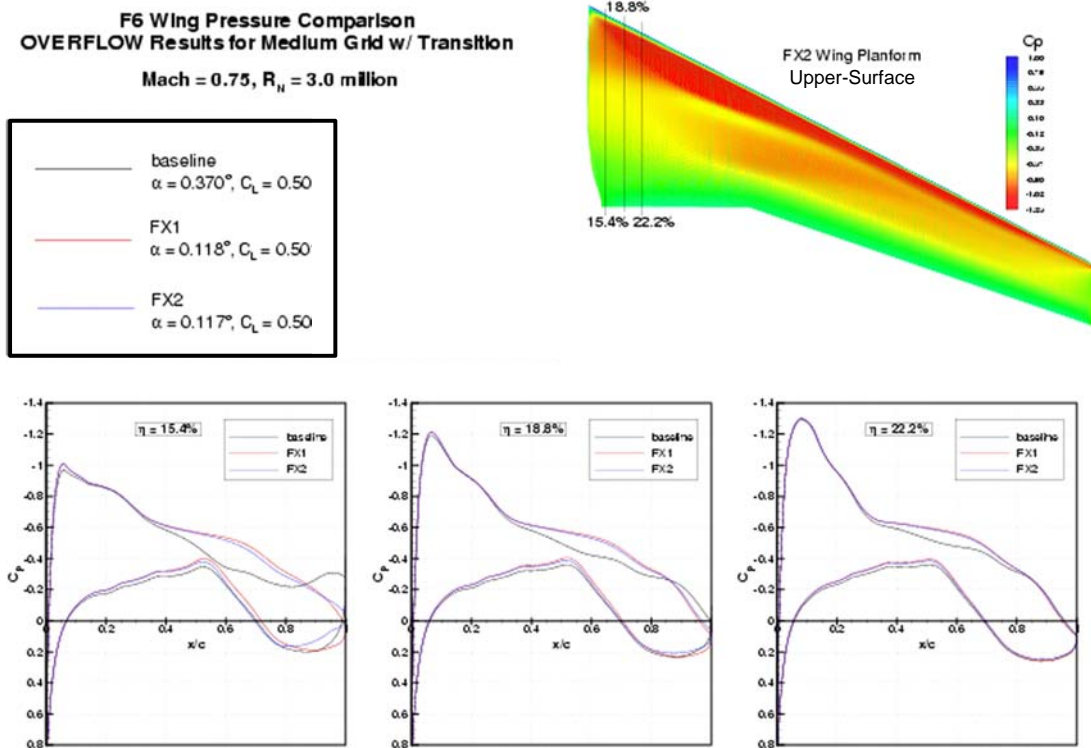


Figure 17: Comparison of Cp Distributions near Side-of-Body.

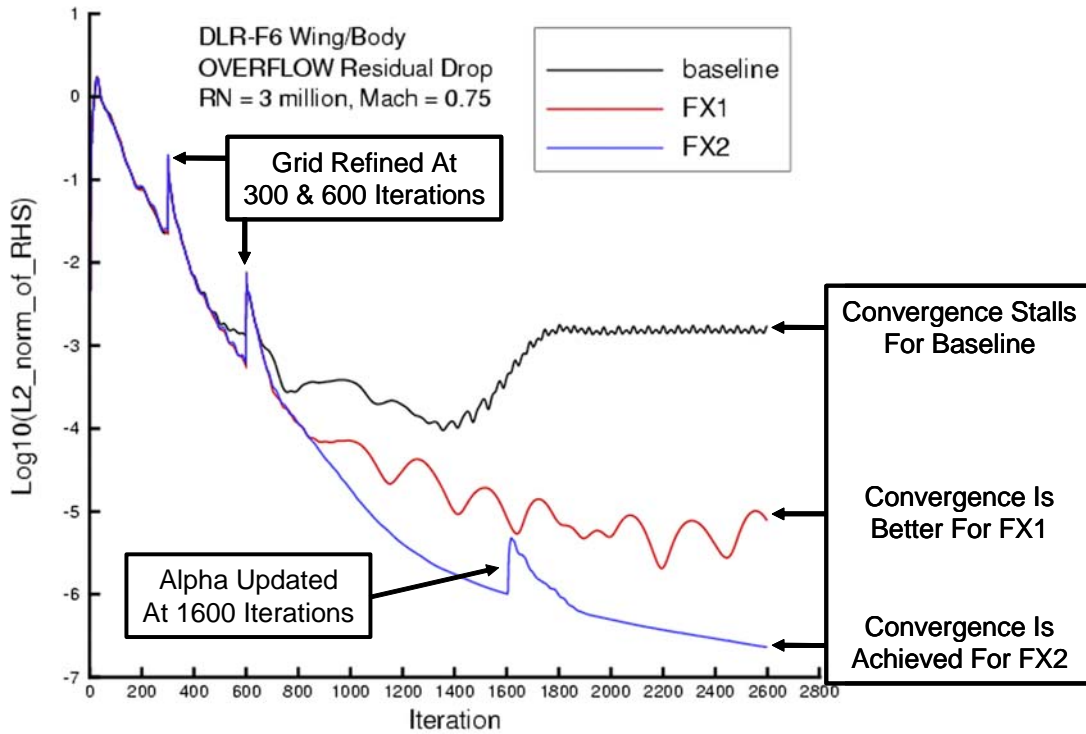


Figure 18: Convergence History of Residuals.

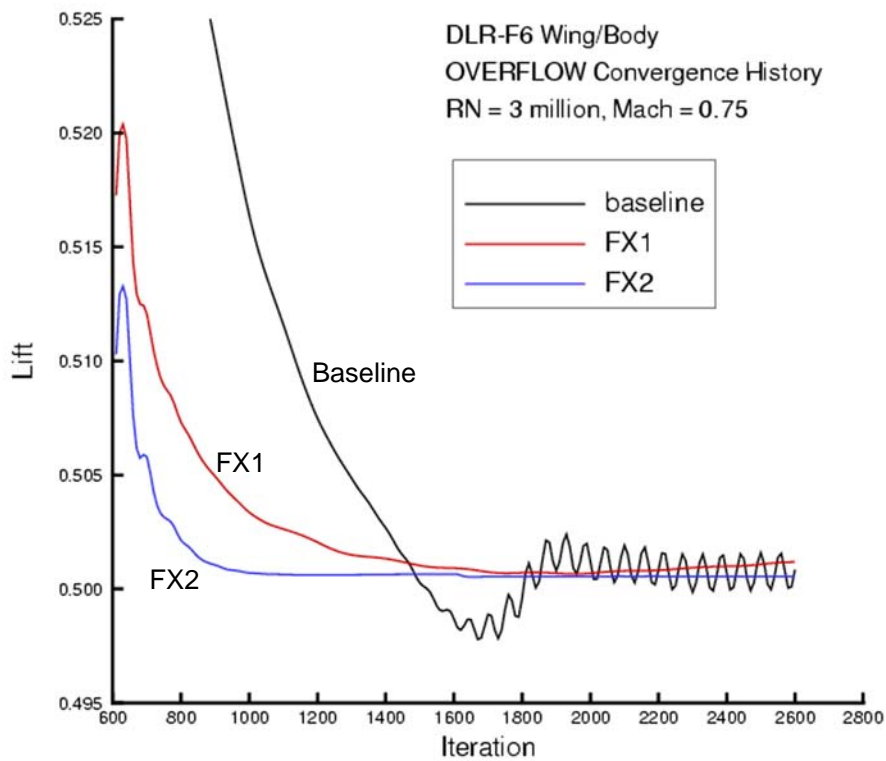


Figure 19: Convergence History of Lift Coefficients.

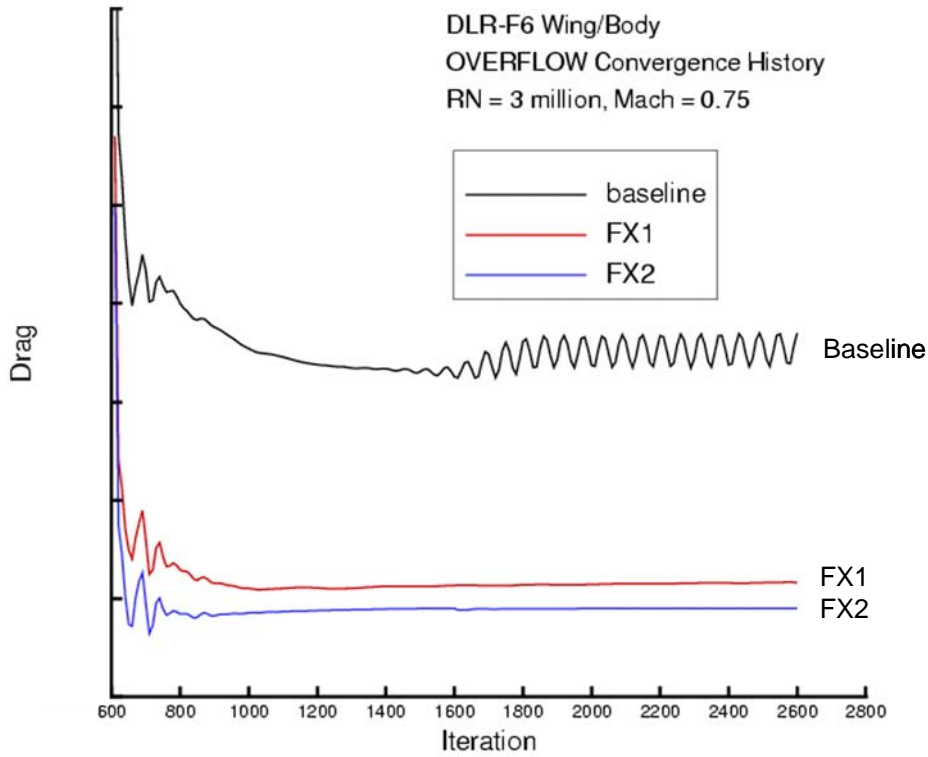


Figure 20: Convergence History of Drag Coefficients.

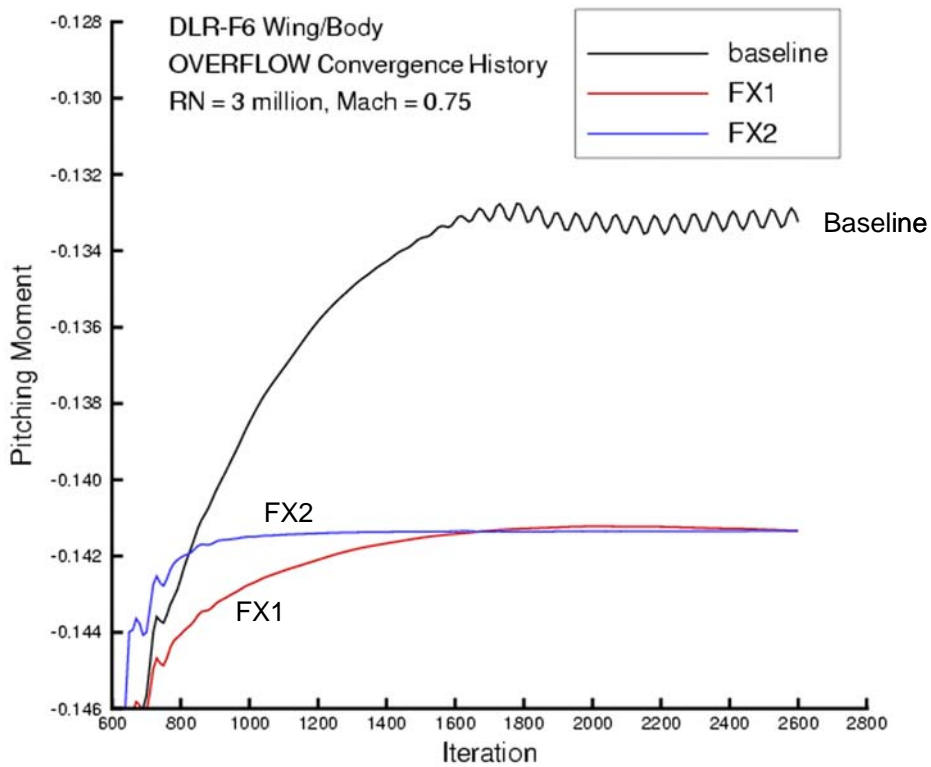


Figure 21: Convergence History of Pitching-Moment Coefficients.